Supplementary Information (SI) for Chemical Science.

This journal is © The Royal Society of Chemistry 2024

Electronic Supplementary Information

Efficient energy transfer from organic triplet states to Mn^{2+} dopants for dynamic lifetime-tunable multicolor afterglow in 1D hybrid cadmium chloride

Ke Zhang,[a] Zhikai Qi,[a,*] Nan Zhang,[a] Xingxing Zhao,[a] Yanli Fan,[a] Long Sun,[b] Guojun Zhou [a], Shi-Li Li [a] and Xian-Ming Zhang[a,c,*]

[a] Key Laboratory of Magnetic Molecules & Magnetic Information Materials (Ministry of Education), School of Chemistry and Material Science, Shanxi Normal University, Taiyuan 030031, P. R. China. E-mail: qizk@sxnu.edu.cn, zhangxm@sxnu.edu.cn.

[b] Department of Chemistry, Changzhi Universtiy, Changzhi 046011, P. R. China.

[c] College of Chemistry & Chemical Engineering, Key Laboratory of Interface Science and Engineering in Advanced Material, Taiyuan University of Technology, Taiyuan 030024, P. R. China.

E-mail: qizk@sxnu.edu.cn, zhangxm@sxnu.edu.cn.

1. Experimental section

1.1 Reagents. The chemicals used in this study include N-benzylpiperidone (NBP, $C_{12}H_{15}NO$, 99%, Aladdin, Shanghai, China), cadmium chloride hemidihydrate ($CdCl_2 \cdot 5/2H_2O$, 99%, Kermel Tianjing China), manganese dichloride tetrahydrate ($MnCl_2 \cdot 4H_2O$, Kermel Tianjing China), hydrochloric acid (HCl, 36%-38%, YongDa, Tianjing, China), and ethanol (C_2H_5OH, 99.7%, Tianjin Guangfu, China). All reagents were procured commercially and used without further purification to synthesize the metal halide hybrid materials.

1.2 Synthesis of NBP-Cd: $CdCl_2 \cdot 2.5H_2O$ (0.228 g, 1 mmol) and **NBP** (180 μL, 1 mmol) were first dissolved in ethanol (4 ml). The solution was acidified by adding hydrochloric acid (1 mL) and stirred for 30 min until the solid was completely dissolved, yielding a clear aqueous solution. The solution was left to stand at room temperature and over the course of a few days, slow evaporation resulted in the formation of tiny rod-shaped crystals. For the synthesis of doped samples, **NBP-Cd:*x*Mn^{2+}** (where x represents the doping level), the feed ratio of $MnCl_2$ and $CdCl_2$ was used to determine the doping level. For example, to prepare **NBP-Cd:10%Mn^{2+}**, 0.1 mmol of $MnCl_2 \cdot 4H_2O$ and 0.9 mmol of $CdCl_2 \cdot 2.5H_2O$ were selected. The remaining experimental procedure was identical to that used for the synthesis of the undoped sample.

1.3 Synthesis of amorphous NBP: NBP (18 μL, 0.1 mmol) was dissolved in ethanol (1 ml) and acidified by adding hydrochloric acid (0.1 mL). The mixture was stirred for 30 min until the NBP was completely dissolved. The resulting solution was dripped onto a watch glass, covered with plastic wrap punctured with 10-15 small holes, and placed in an oven at 60 °C. After standing for 1-2 days, amorphous NBP was obtained.

1.4 X-ray Crystallographic Study. Single-crystal X-ray diffraction data of **NBP-Cd** and **NBP-Cd:*x*Mn^{2+}** crystals were collected using an Agilent single crystal diffractometer with Mo Kα radiation (λ=0.71073 Å). The crystal structure of NBP-Cd was solved directly using the SHELXL-97 package on the Olex2 software. This was followed by full matrix least-squares minimi sation of F^2 with anisotropic refinement of Cd, Cl, O, C and N atoms. In theory, all of the H atoms in the organic cations are generated on top of C, O and N atoms using isotropic refinement. Table S1 and Table S2 give crystallographic data for some of the bond lengths and angles in the structures.

1.5 Photoluminescence measurements. The photoluminescence (PL) measurements of **NBP-Cd** and **NBP-Cd:*x*Mn^{2+}**, involving excitation spectrum, temperature-dependent PL spectra, and time-resolved decay data, were performed on an Edinburgh FLS-980 fluorescence spectrometer with a picosecond pulsed diode laser. PLQY was achieved using FLS-920 spectrofluorometer equipped with an integrating sphere. The equation: $\eta_{QE} = I_S / (E_R - E_S)$ was used to calculate PLQY, where I_S stands for the emission spectra of the compound, E_R is the spectra of the excitation light of the empty integrated sphere, and E_S is the excitation spectra of the excited sample. The CIE chromaticity coordinates were calculated using the CIE calculator software based on the emission spectra. For the kinetic lifetime measurement, the excitation source continuously irradiates the sample from ~ 2 s to ~ 6 s, and the decay process starts at the 6th second.

1.6 Characterization. TU-1950 UV spectrometer was used to record the UV-vis absorption curves of these benchmark material and undoped derivates at ambient condition, where the standard reference was $BaSO_4$. Powder X-ray diffraction (XRD) measurements were measured at 40 kV and 100 mA on a Rigaku D/Max-2500 diffractometer with Cu Kα radiation, and the powder diffraction patterns were collected in the 2θ range of 5° to 50° with a step size of 0.02 min^{-1}. TGA measurement was carried out on a NETZSCH STA 449F3 thermal analyzer under N_2 at a heating rate of 10 °C/min. The DSC data were measured on a DSC214 Polyma Differential Scanning Calorimeter. The content of Mn/ Cd was measured by the ICP analysis with an ICP Analyzer (Avio 220 MAX).

1.7 DFT calculations. First-principles calculations were performed by DFT using Vienna ab-initio simulation package (VASP, version 5.4), in which all-electron information was reconstructed by projected augmented-wave (PAW) pseudopotentials. The exchange-correlation energy was treated by the Perdew-Burke-Ernzerhof (PBE) exchange-correlation functional in the scheme of generalized gradient approximation. The kinetic energy cutoff for all cases was determined to be 520 eV. The convergence thresholds for the electronic calculations and ionic relaxations were chosen as 10^{-6} eV and 0.01 eV/Å, respectively. The standard Monkhorst-Pack *k*-point grids with density of 0.1 Å^{-1} were used for Brillouin zone sampling. The valence electron configurations applied in this work were treated as Cd ($5s^2 4p^6$), C ($2s^22p^2$), Cl ($3s^23p^5$), N ($2s^22p^3$), O ($2s^22p^3$), and H ($1s^1$). The highest occupied molecular orbitals (HOMO), as well as lowest unoccupied molecular orbitals (LUMO) for 1D Cd-based halide hybrid in this work, were also carried out by DFT calculations with orbital occupancies. In the first-principles calculations of Mn^{2+}-doped NBP-Cd, the model used was obtained by replacing one Cd^{2+} ion with a Mn^{2+} ion within the unit cell. The doping ratio is 12.5%, approaching to that of the actual doping ratio (12%) for the NBP-Cd:20% sample.

1.8 Hirshfeld surface analysis. Hirshfeld surfaces and related two-dimensional (2D) fingerprints of NBP^+ cations in the asymmetric unit of **NBP-Cd** was calculated using Crystal Explorer 21.5 program with inputting structure file in CIF format. In this work, all the Hirshfeld surfaces were generated using a standard (high) surface resolution. The three-dimensional (3D) Hirshfeld surfaces and 2D fingerprint plots are unique for any crystal structure. The intensity of intermolecular interaction is mapped onto the Hirshfeld surface by using the respective red-blue-white scheme: where the white or green regions exactly correspond to the distance of van der Waals contact, the blue regions correspond to longer contacts, and the red regions represent closer contacts. In 2D fingerprint plots, each point represents an individual pair (d_i, d_e), reflecting the distances to the nearest atom inside (d_i) and outside (d_e) of the Hirshfeld surface, and the frequency of occurrence for these points correspond to the color from blue (low), through green, to red (highest). The normalized contact distance d_{norm} is based on d_e, d_i and the van der Waals (vdW) radii of the two atoms external (r_e^{vdW}) and internal (r_i^{vdW}) to the surface:

$$d_{norm} = \frac{d_i - r^{vdW}}{r^{vdW}_{i}} + \frac{d_e - r}{r^{vdW}_{e}}$$

d_{norm} surface is used for the identification of very close intermolecular interactions. The value of d_{norm} is negative or positive when intermolecular r contacts are shorter or longer than r^{vdW}, respectively.

2. Supporting figures

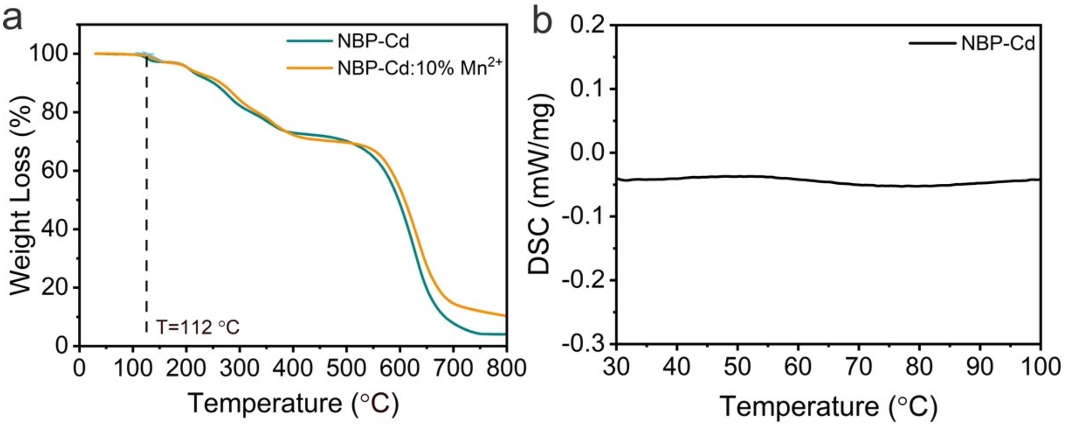

Fig. S1 (a) Thermogravimetric curves of NBP-Cd and NBP-Cd:10%Mn^{2+}. (b) DSC curve of NBP-Cd.

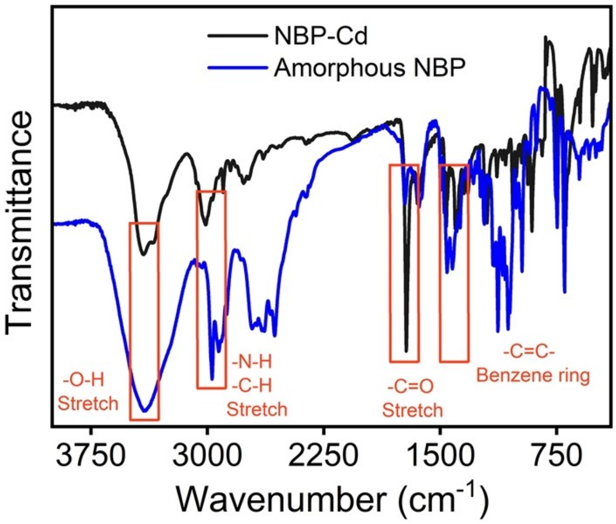

Fig. S2 FT-IR spectrum of **NBP-Cd** and amorphous **NBP**.

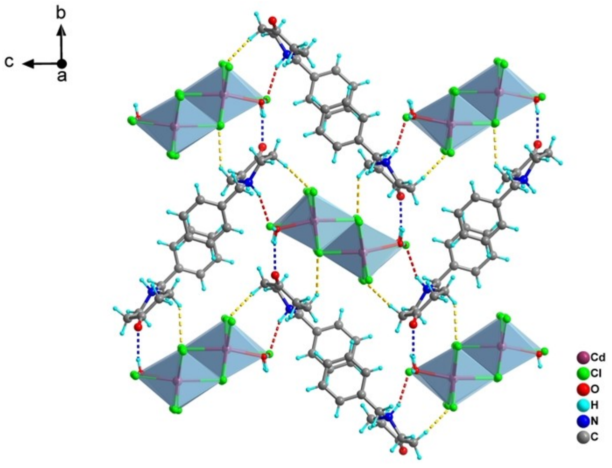

Fig. S3 Hydrogen bonding in **NBP-Cd**.

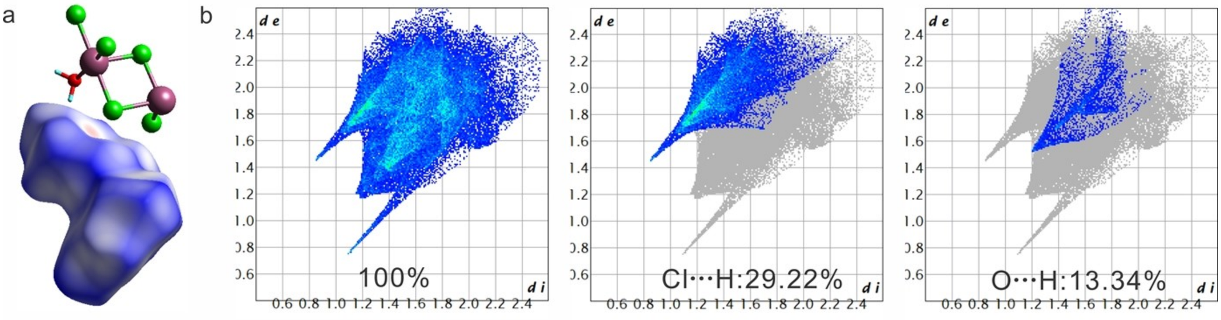

Fig. S4 3D Hirshfeld surface and 2D fingerprint plotting for the NBP$^+$ cations.

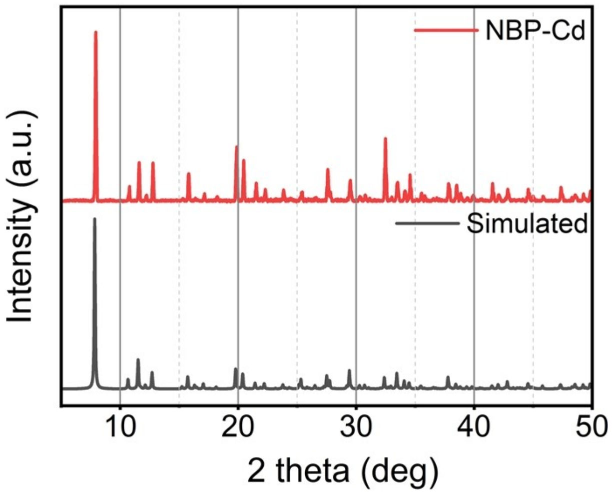

Fig. S5 Experimental and simulated powder XRD data of **NBP-Cd**.

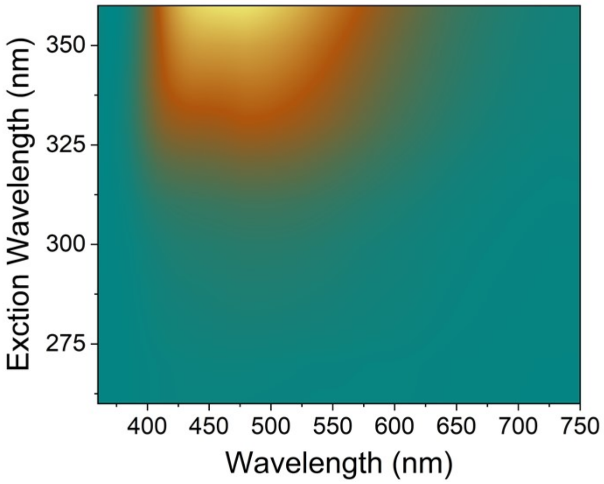

Fig. S6 3D mapping spectrum of **NBP-Cd** under excitation in the range of 260nm to 360nm.

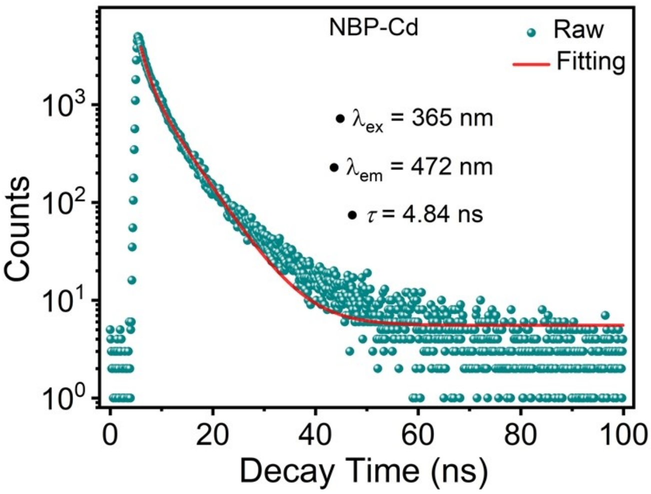

Fig. S7 Time-resolved PL decay data and fitting line for emission peak at 472 nm in **NBP-Cd**.

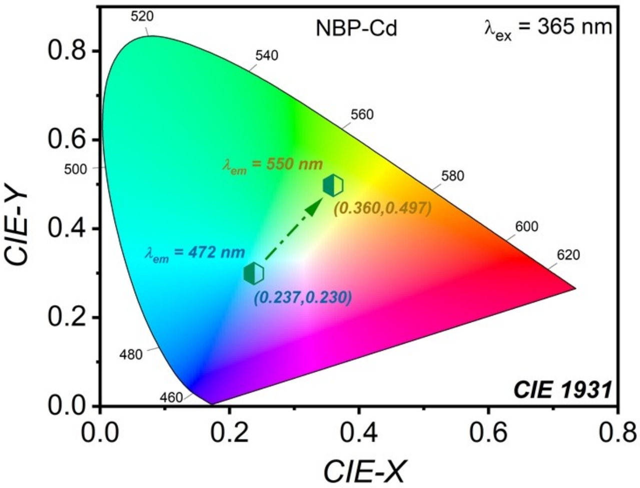

Fig. S8 CIE chromaticity diagram corresponding to the prompt and delayed spectrum of **NBP-Cd** under excitation at 365 nm.

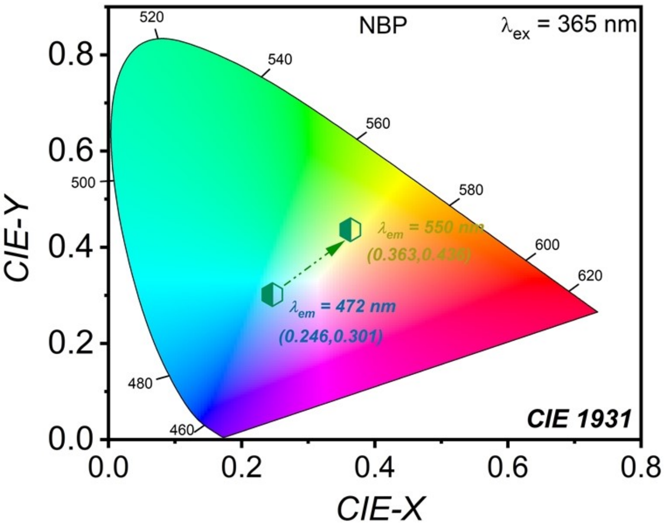

Fig. S9 CIE chromaticity diagram corresponding to the prompt and delayed spectrum of amorphous **NBP** under excitation at 365 nm.

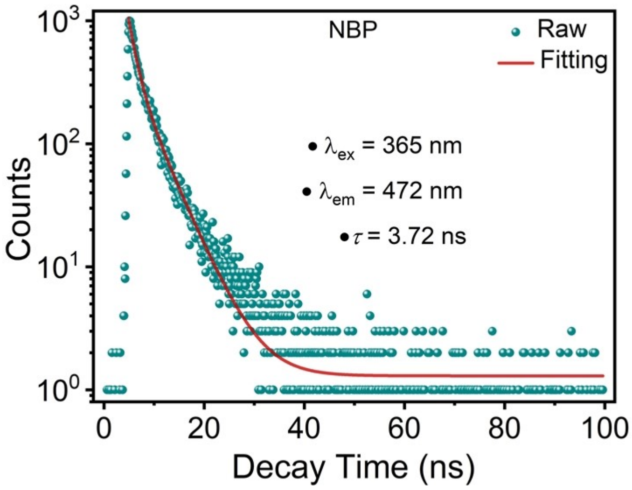

Fig. S10. Time-resolved PL decay and fitting of the amorphous **NBP** at 472 nm.

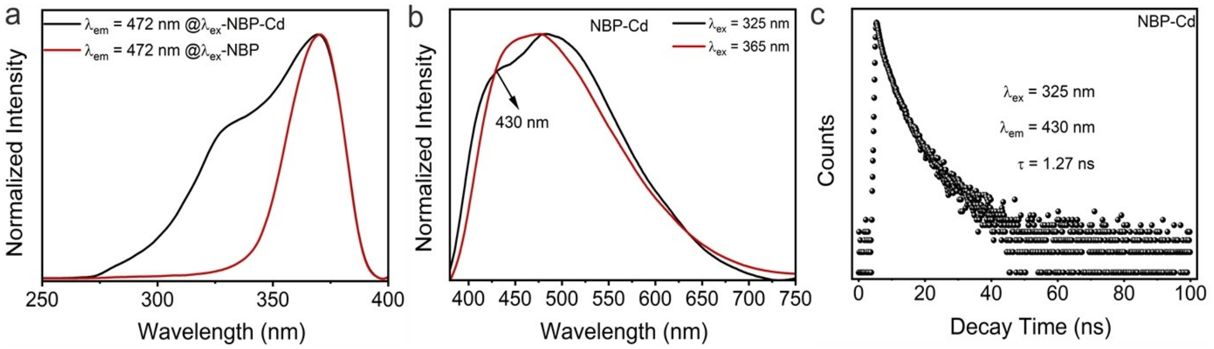

Fig. S11 (a) PLE spectra of **NBP-Cd** and the amorphous **NBP** corresponding the emission peak at 472 nm. (b) Emission spectra of NBP-Cd under excitations at 325 nm and 365 nm. (c) PL lifetime of **NBP-Cd** under excitation at 325 nm.

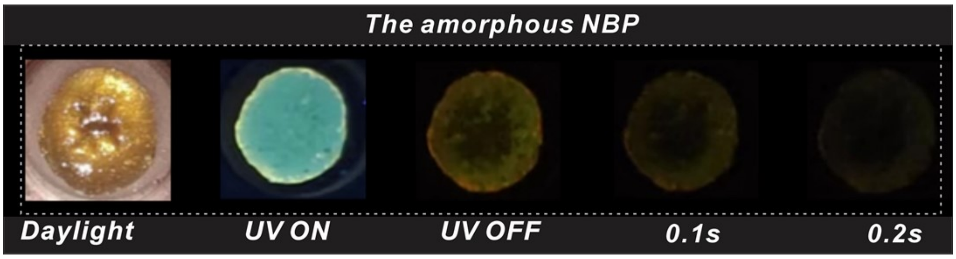

Fig. S12 Photographs of the amorphous **NBP** before and after cessation of the 365 nm irradiation.

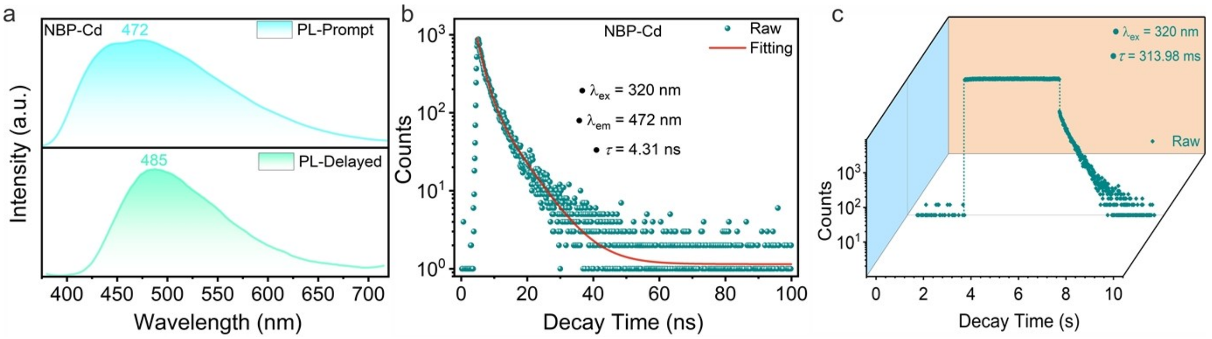

Fig. S13 (a) Prompt and delayed PL spectra for **NBP-Cd** under excitation at 320 nm. (b) Time-resolved PL decay and fitting of **NBP-Cd** at 472 nm. (c) Kinetic lifetime lifetimes of **NBP-Cd** under excitation at 320 nm and the emission at 485 nm.

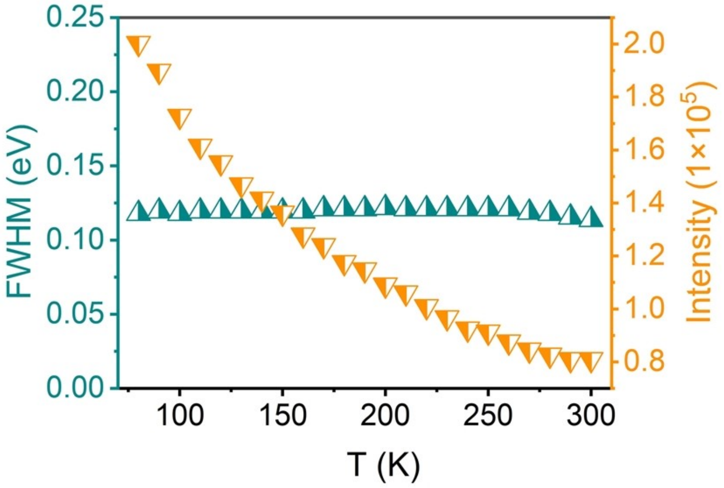

Fig. S14 Band width and peak intensity of **NBP-Cd** in the range of 80−300 K.

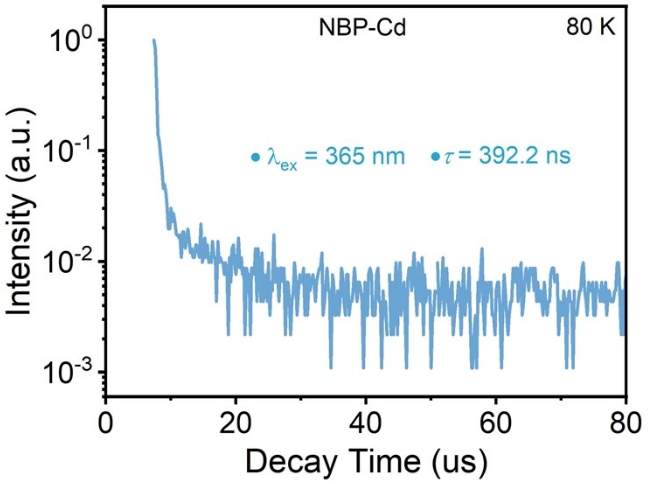

Fig. S15 Time-resolved PL decay of **NBP-Cd** at 77K under 365 nm excitation.

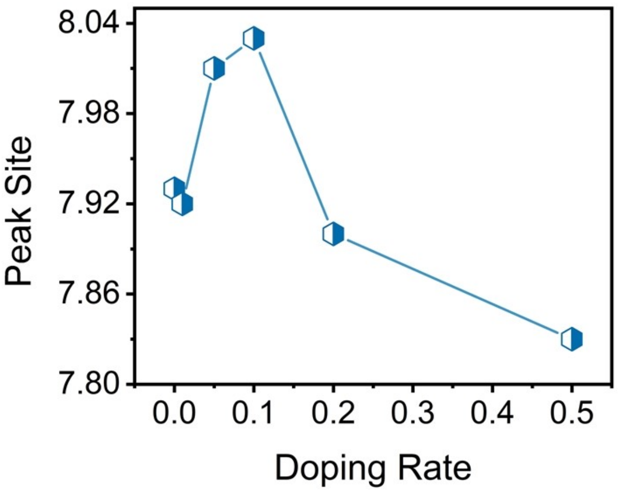

Fig. S16 The variation in the positions of the diffraction peaks in Powder X-ray Diffraction (PXRD) as a function of doping concentration within the 2θ range of 7.5° to 8.5°.

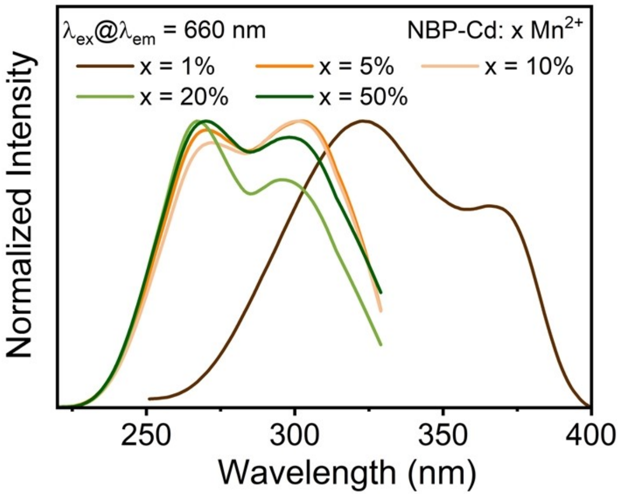

Fig. S17 PLE spectra of NBP-Cd:xMn^{2+} corresponding to the emission peak at 660 nm.

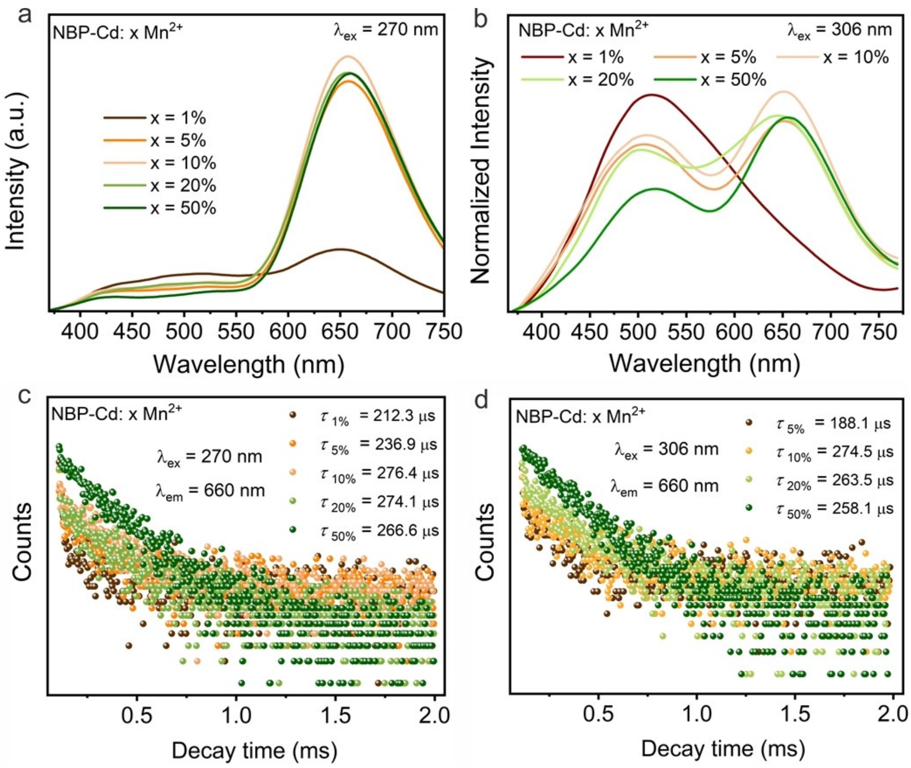

Fig. S18 Emission spectra of NBP-Cd:xMn^{2+} upon excitation at (a) 270 nm and 306 nm. Decay curves of NBP-Cd:xMn^{2+} upon excitation at (c) 270 nm and 306 nm.

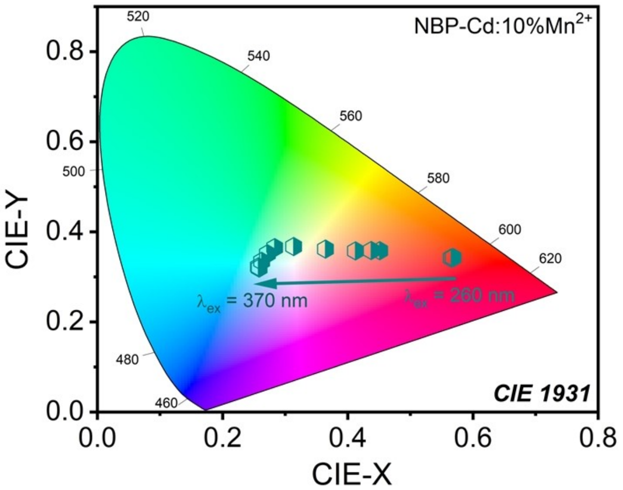

Fig. S19 CIE chromaticity diagram of **NBP-Cd:10%Mn^{2+}** under photoexcitation from 260 nm to 360 nm.

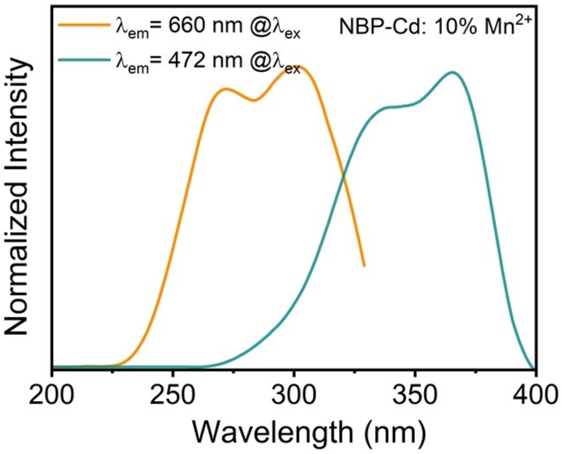

Fig. S20 PLE spectra of **NBP-Cd:10%Mn^{2+}** at different emission peaks.

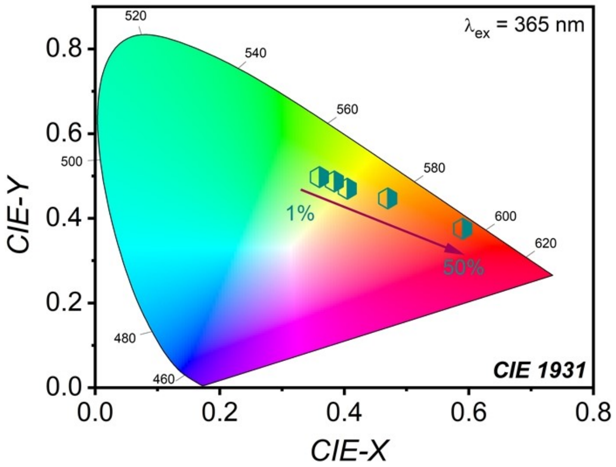

Fig. S21 CIE chromaticity diagram of **NBP-Cd:*x*Mn^{2+}** (*x* = 1%, 5%, 10%, 20%, 50%) under excitation at 360 nm.

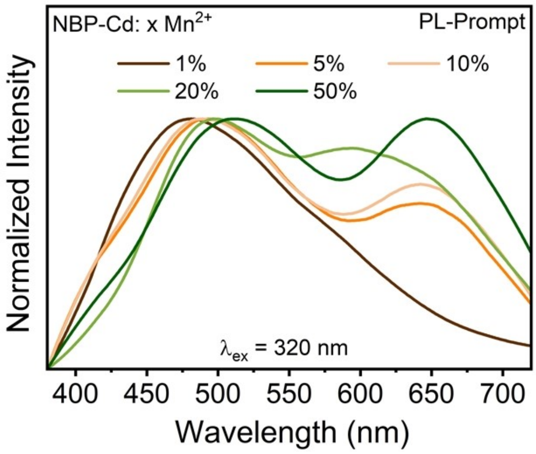

Fig. S22 PL spectra of NBP-Cd:xMn^{2+} under 320 nm excitation.

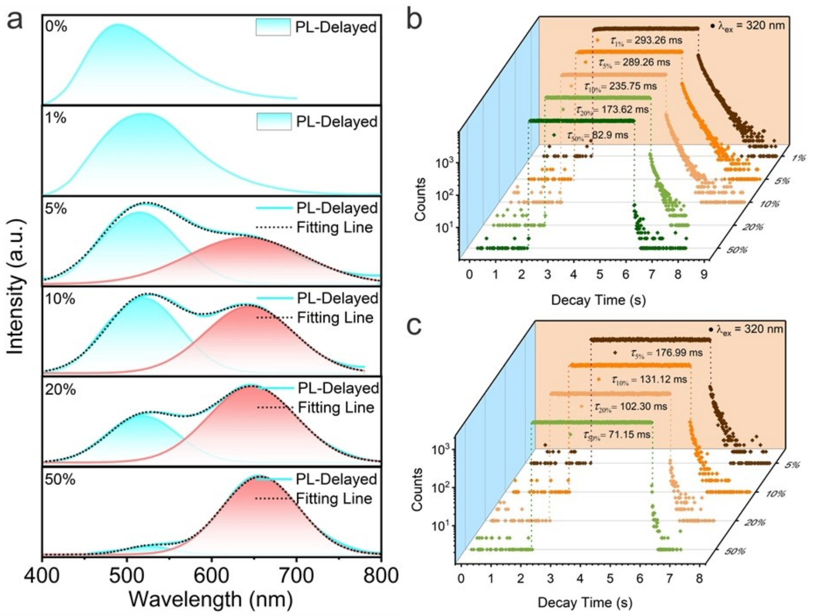

Fig. S23 (a) Delayed emission spectra and corresponding kinetic decay curves of emission peaks at (b) 510 nm and (c) 660 nm in NBP-Cd:xMn^{2+} under 320 nm excitation.

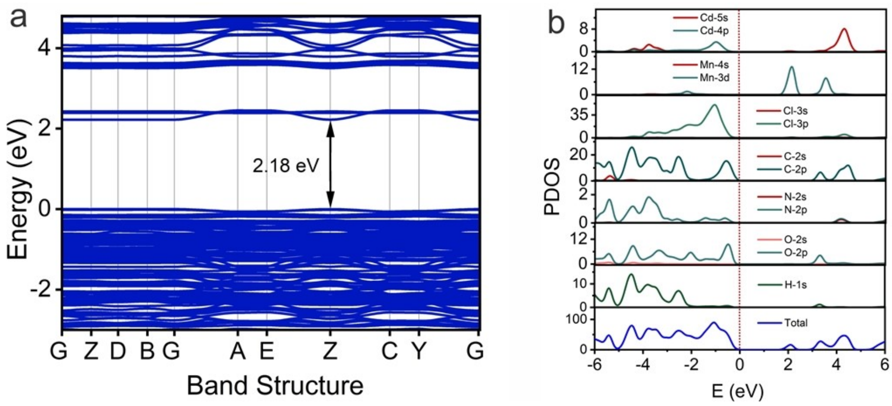

Fig. S24 (a) Band structure and (b) PDOS of NBP-Cd:20%Mn^{2+}.

3. Supporting tables

Table S1. Crystal data and structure refinement for **NBP-Cd**.

Empirical formula	$C_{12}H_{18}Cd_2Cl_5NO_2$
Formula weight	610.32
Temperature/K	293(2)
Crystal system	monoclinic
Space group	$P2_1/c$
a/Å	7.5573(8)
b/Å	15.3477(16)
c/Å	16.6274(18)
α/°	90
β/°	94.566(2)
γ/°	90
Volume/Å^3	1922.4(4)
Z	4
ρ_{calc}g/cm^3	2.109
μ/mm^{-1}	2.910
F(000)	1176.0
Crystal size/mm^3	0.1 × 0.1 × 0.05
Radiation	Mo K_α ($\lambda = 0.71073$)
2Θ range for data collection/°	5.408 to 56.612
Reflections collected	21992
Independent reflections	4754 [$R_{int} = 0.0567$, $R_{sigma} = 0.0449$]
Data/restraints/parameters	4754/0/201
Final R indexes [I>=2σ (I)]	$R_1 = 0.0510$, $wR_2 = 0.1390$
Final R indexes [all data]	$R_1 = 0.0689$, $wR_2 = 0.1480$
Largest diff. peak/hole / e Å^{-3}	1.92/-1.00

$^aR_1 = \sum||F_o|-|F_c||/\sum|F_o|$. $^bwR_2 = [w(F_o^2-F_c^2)^2/w(F_o^2)^2]^{1/2}$

Table S2. Selected bond distances of **NBP-Cd**.

Atom-Atom	Length/Å	Atom-Atom	Length/Å
Cd1-Cl1	2.6281(16)	Cd2-Cl1a	2.6726(16)
Cd1-Cl1c	2.7314(16)	Cd2-Cl4	2.6577(16)
Cd1-Cl4	2.6567(16)	Cd2-Cl4a	2.7670(16)
Cd1-Cl2	2.5481(17)	Cd2-Cl5	2.5485(18)
Cd1-Cl3	2.5509(18)	Cd2-Cl2b	2.5735(17)
Cd1-O1	2.325(5)	Cd2-Cl3	2.5667(17)

Symmetric code: (a) 1-*x*, 1-*y*, 1-*z*; (b) -1+*x*, +*y*, +*z*; (c) 2-*x*, 1-*y*, 1-*z*

Table S3. Selected bond angle of **NBP-Cd**.

Atom-Atom-Atom	Angle/°	Atom-Atom-Atom	Angle/°
Cl1a-Cd2-Cl4a	81.84(5)	O1-Cd1-Cl3	97.24(15)
Cl4-Cd2-Cl1a	89.87(5)	Cd2a-Cl1-Cd1c	87.59(5)
Cl4-Cd2-Cl4a	81.58(5)	Cd1-Cl1-Cd2a	98.14(5)
Cl5-Cd2-Cl1a	89.34(6)	Cd1-Cl1-Cd1c	95.23(5)
Cl5-Cd2-Cl4a	170.80(6)	Cd2-Cl4-Cd2a	98.42(5)
Cl5-Cd2-Cl4	95.86(6)	Cd1-Cl4-Cd2a	95.17(5)
Cl5-Cd2-Cl2b	92.80(6)	Cd1-Cl4-Cd2	91.92(5)
Cl5-Cd2-Cl3	94.05(6)	Cd1-Cl2-Cd2d	93.82(6)
Cl2b-Cd2-Cl1a	89.25(5)	Cd1-Cl3-Cd2	96.58(6)
Cl2b-Cd2-Cl4a	89.72(6)	Cl2-Cd1-Cl1	90.96(6)
Cl2b-Cd2-Cl4	171.29(6)	Cl2-Cd1-Cl4	175.48(6)
Cl3-Cd2-Cl1a	174.58(5)	Cl2-Cd1-Cl3	96.14(6)
Cl3-Cd2-Cl4	85.58(5)	Cl3-Cd1-Cl1c	175.21(5)
Cl3-Cd2-Cl41	94.55(6)	Cl3-Cd1-Cl1	96.33(6)
Cl3-Cd2-Cl2b	94.80(6)	Cl3-Cd1-Cl4	85.92(5)
Cl1-Cd1-Cl1c	84.77(5)	O1-Cd1-Cl1c	81.38(15)
Cl1-Cd1-Cl4	84.81(5)	O1-Cd1-Cl1	165.86(15)
Cl4-Cd1-Cl1c	89.55(5)	O1-Cd1-Cl4	92.23(15)
Cl2-Cd1-Cl1c	88.49(5)	O1-Cd1-Cl2	91.50(15)

Symmetric code: (a) 1-*x*, 1-*y*, 1-*z*; (b) -1+*x*, +*y*, +*z*; (c) 2-*x*, 1-*y*, 1-*z*; (d) 1+*x*, +*y*, +*z*

Table S4. H bonds of **NBP-Cd**.

D-H···A	d(D-H)/Å	d(H-A)/Å	d(D-A)/Å	D-H-A/°
O1-**H1A**···**O2**	0.86	1.99	2.832(10)	167.4
O1-**H1B**···**Cl5a**	0.86	2.37	3.218(6)	171.8
N1-**H1**···**Cl5b**	0.98	2.35	3.265(6)	155.9
C4-**H4A**···**Cl3b**	0.97	2.84	3.476(9)	123.9

Symmetric code: (a) 1+*x*, +*y*, +*z*; (b) 1-*x*, -1/2+*y*, 3/2-*z*

Table S5. PLQY of **NBP-Cd:*x*Mn^{2+}** under excitation at 254 nm and 270 nm.

Compound	**NBP-Cd: *x*Mn^{2+}**				
	1%	5%	10%	20%	50%
PLQY (254 nm)	2.7%	13%	31.1%	30.7%	20.6%
PLQY (270 nm)	3.6%	20.1%	40.5%	39.17%	34.9%